

# Effect of Hydrogen and Defects on Deformation and Failure of Austenitic Stainless Steel



Eugene Ogosi, Amir Siddiq, Umair Bin Asim, and Mehmet E. Kartal

**Abstract** Austenitic stainless steels are used for a variety of applications and could suffer degradation of properties when exposed to hydrogen. The performance of these steels are also dependent on crystallographic texture which in practice is a factor influenced by manufacturing processes. A study has been performed using a crystal plasticity based finite element model to understand the effect of crystal orientation with respect to loading direction for FCC single crystals in both hydrogenated and non-hydrogenated environment. The purpose of the study is to understand the effect of crystal orientation on how hydrogen influences plastic deformation and void growth. Simulations have been performed for a variety of stress triaxialities, Lode parameters and hydrogen concentrations. It is observed that initial crystal orientation has a varied effect on the influence hydrogen has on plastic deformation and void growth. Hydrogen in trap distribution at various stages of the deformation process was also found to be influenced by initial crystal orientation. Hydrogen affects the evolution of crystal rotation during deformation but was not found to significantly affect the general pattern of crystal orientation evolution.

**Keywords** Crystal plasticity · Crystal orientation · Hydrogen embrittlement · Void growth · Plastic deformation

## 1 Introduction

Manufacturing processes are used to form steel into useful products. The mechanical and corrosion resistant properties are known to be strongly dependent on the

---

E. Ogosi

Apache North Sea, Prime Four Business Park Kingswells, Aberdeen AB15 8PU, UK

E. Ogosi · A. Siddiq (✉) · M. E. Kartal

School of Engineering, University of Aberdeen, Aberdeen AB24 3FX, UK

e-mail: [amir.siddiq@abdn.ac.uk](mailto:amir.siddiq@abdn.ac.uk)

U. B. Asim

Department of Materials Science and Engineering, Texas A&M University, College Station, TX 77843, USA

texture of the material inherited during manufacture [1]. The crystallographic texture of steel has been found to affect hydrogen resistant properties [2, 3]. Hydrogen has a deleterious effect on steel and since the nineteenth century, its effect have been subject to many studies and reviews [4–7]. Specifically, experimental work has been performed on hydrogen embrittlement of austenitic stainless steel [8, 9]. The hydrogen enhanced localized plasticity (HELP) theory is used to explain how hydrogen, in steel undergoing deformation, enhances dislocation motion at a microscopic scale by elastic shielding of dislocation interactions with other dislocations and microstructural structures [7, 10]. In face centred cubic (FCC) metals, with relatively low hydrogen diffusivity, this has been observed to lead to local dislocation pile ups [11, 12] and increased plastic flow properties [13]. Crystal orientation in relation to the rolling, normal and transverse directions have been found to influence materials resistance to hydrogen induced cracking for both face centred cubic (FCC) and body centred cubic (BCC) crystal materials [14, 15]. Crystal orientation parallel to the normal direction was found to improve resistance to hydrogen induced cracking [14, 15]. Potirniche et al. investigated the effect of crystal orientation on void growth of an FCC crystals without hydrogen influence [16]. They performed 2D finite element simulations using a crystal plasticity based model to understand the effects of crystal orientation and loading biaxiality on void characteristics. Results from these studies showed that crystal orientation had a significant effect on void growth. Asim et al. [17] previously observed that crystal orientation has significant impact on the void growth and that this effect reduces with increasing triaxiality. Activation of slip systems plays an important part in the dependence of plastic deformation on loading direction and crystal orientation. It was reported by Michler and colleagues [18] that austenite phase stability is not a guarantee that stainless steel is resistance to hydrogen embrittlement. They performed experiments on stable austenitic stable steels and observed hydrogen embrittlement even when there was no evidence of phase transformation to martensite. Crystal orientation was found to affect plastic slip localization, void growth and its shape evolution. Hua et al. performed experimental studies to understand the effect of crystal orientation on hydrogen diffusion using specialized microscopy and electron back scatter diffraction (EBSD) [19]. They found that that hydrogen diffusion had a strong dependence on crystal orientation. Hydrogen mobility in 304 stainless steel crystal grains were found to be higher in (111) oriented grains when compared with (001) and (101) oriented grains. Depending of crystal orientation, it was observed that hydrogen affected the plastic deformation differently [20]. This was explained by the difference in deformation mechanism viz a viz slip and twinning experienced and the effect of applied stress on splitting of dislocations. In this work, we investigate the effects of initial crystal orientation on how hydrogen affects the properties of austenitic stainless steels and study the effects of hydrogen on crystallographic rotation evolution. Simulations have been performed for a variety of stress triaxialities (0.8, 1, 1.5, 2 & 3) and Lode parameters ( $-1, 0$  &  $1$ ). The model formulation is presented in Sect. 2. Methodology is explained in Sect. 3. Results are presented in Sect. 4. Conclusions are presented in Sect. 5.

## 2 Crystal Plasticity Model with Hydrogen Effects

### 2.1 Crystal Plasticity Theory

A crystal plasticity model [21, 22] has been extended to include hydrogen influence [23]. A brief summary of the model formulation is presented. Deformation gradient is expressed as a product of its elastic  $F^e$ , hydrogen  $F^h$  and elastic  $F^p$  components [24];

$$\mathbf{F} = \mathbf{F}^e \mathbf{F}^h \mathbf{F}^p \quad (1)$$

Marin's formulation [21] with a hydrogen component is expressed as:

$$\mathbf{F} = \mathbf{V}_e \mathbf{F}^*, \quad \mathbf{F}^* = \mathbf{R}^e \mathbf{F}^h \mathbf{F}^p \quad (2)$$

$\mathbf{V}_e$  is elastic stretch and  $\mathbf{R}^e$  is rotation. The velocity gradient  $\mathbf{l}$  in the final deformed state is given by;

$$\mathbf{l} = \dot{\mathbf{F}} \mathbf{F}^{-1} \quad (3)$$

$\dot{\mathbf{F}}$  and  $\mathbf{F}^{-1}$  are the rate of change deformation gradient and its inverse. Velocity gradient ( $\tilde{\mathbf{L}}$ ) in an intermediate state with elastic stretch unloaded is given by:

$$\tilde{\mathbf{L}} = \mathbf{V}^{e-1} \mathbf{l} \mathbf{V}^e = \mathbf{V}^{e-1} \dot{\mathbf{V}}^e + \tilde{\mathbf{L}}^* \quad (4)$$

$\mathbf{V}^{e-1}$  is the inverse of stretch.

$$\tilde{\mathbf{L}}^* = \mathbf{R}^e \mathbf{R}^{eT} + \mathbf{R}^e \hat{\mathbf{L}}^h \mathbf{R}^{eT} + \mathbf{R}^e \mathbf{F}^h \bar{\mathbf{L}}^p \mathbf{F}^{h-1} \mathbf{R}^{eT} \quad (5)$$

$\dot{\mathbf{R}}^e$  is the rotation change rate and  $\mathbf{R}^{eT}$  is the transpose of  $\mathbf{R}^e$ . The plastic part of the velocity gradient  $\bar{\mathbf{L}}^p$ , is given by:

$$\bar{\mathbf{L}}^p = \sum \dot{\gamma}^\alpha \bar{\mathbf{s}}^\alpha \otimes \bar{\mathbf{m}}^\alpha \quad (6)$$

$\bar{\mathbf{s}}^\alpha$  is the direction and  $\bar{\mathbf{m}}^\alpha$  is the normal component. Combining (5) and (6):

$$\tilde{\mathbf{L}}^* = \tilde{\mathbf{\Omega}}^e + \hat{\mathbf{L}}^h + \sum_{\alpha=1}^N \dot{\gamma}^\alpha \bar{\mathbf{s}}^\alpha \otimes \mathbf{m}^\alpha \quad (7)$$

$\tilde{\mathbf{\Omega}}^e = \dot{\mathbf{R}}^e \mathbf{R}^{eT}$  is elastic spin.  $\dot{\gamma}^\alpha$  is the rate shear strain.

Sofronis provides an expression for the hydrogen deformation gradient [25]:

$$\mathbf{F}^h = \left(1 + \frac{(c - c_0)\lambda}{3}\right) \mathbf{I} \quad (8)$$

$c_0$  and  $c$  are the initial and final hydrogen concentrations.  $\lambda$  is  $\frac{\Delta V}{V_m}$ ,  $\Delta V$  is volume change and  $V_m$  is atomic volume.

The hydrogen part of the velocity gradient  $\hat{\mathbf{L}}^h$  is:

$$\hat{\mathbf{L}}^h = \dot{\mathbf{F}}^h \cdot \mathbf{F}^{h-1} = \frac{1}{3} \left[ \frac{3\lambda}{3 + (c - c_0)} \right] (c) \dot{c} \mathbf{I} \quad (9)$$

The Second Piola–Kirchhoff stress tensor,  $\tilde{\mathbf{S}}$  is:

$$\tilde{\mathbf{S}} = \tilde{\mathbf{C}}^e : \tilde{\mathbf{E}}^e \quad (10)$$

$\tilde{\mathbf{C}}^e$  and  $\tilde{\mathbf{E}}^e$  are the elasticity and Green–Lagrange strain tensors. Deformation tensor splits into a symmetric,  $\tilde{\mathbf{D}}$ , and skew,  $\tilde{\mathbf{W}}$  part:

$$\tilde{\mathbf{D}} = \mathbf{V}^{eT} \mathbf{d} \mathbf{V}^e = \tilde{\mathbf{E}}^e + \left[ \text{sym}(\tilde{\mathbf{C}}^e \tilde{\mathbf{\Omega}}^e) + \sum_{\alpha=1}^N \dot{\gamma}^\alpha \text{sym}(\tilde{\mathbf{C}}^e \tilde{\mathbf{Z}}^\alpha) \right] \quad (11)$$

$$\tilde{\mathbf{W}} = \mathbf{V}^{eT} \mathbf{w} \mathbf{V}^e = \text{skew}(\mathbf{V}^{eT} \dot{\mathbf{V}}^e) + \left[ \text{skew}(\tilde{\mathbf{C}}^e \tilde{\mathbf{\Omega}}^e) + \sum_{\alpha=1}^N \dot{\gamma}^\alpha \text{skew}(\tilde{\mathbf{C}}^e \tilde{\mathbf{Z}}^\alpha) \right] \quad (12)$$

where  $\tilde{\mathbf{C}}^e = \mathbf{R}^e \tilde{\mathbf{C}}^e \mathbf{R}^{eT}$  and  $\tilde{\mathbf{Z}}^\alpha = \tilde{s}^\alpha \otimes \tilde{m}^\alpha$ .

Plastic slip evolution is given as:

$$\dot{\gamma}^\alpha = \dot{\gamma}_0^\alpha \left[ \frac{|\boldsymbol{\tau}^\alpha|}{\kappa_s^\alpha} \right]^{\frac{1}{m}} \text{sign}(\tau^\alpha) \quad (13)$$

$\dot{\gamma}^\alpha$  is strain rate in  $\alpha$ ,  $\dot{\gamma}_0^\alpha$  is the reference strain rate,  $\kappa_s^\alpha$  is the current crystal strength of  $\alpha$ ,  $\tau^\alpha$  is resolved stress and  $m$  is rate sensitivity. The slip system hardens as follows;

$$\dot{\kappa}_s^\alpha = h_0 \left( \frac{\kappa_{s,S}^\alpha - \kappa_s^\alpha}{\kappa_{s,S}^\alpha - \kappa_{s,0}^\alpha} \right) \sum_{\alpha=1}^N |\dot{\gamma}^\alpha|, \kappa_{s,S}^\alpha = \kappa_{s,S0}^\alpha \left[ \frac{\sum_{\alpha} |\dot{\gamma}^\alpha|}{\dot{\gamma}_{s0}^\alpha} \right]^{1/m'} \quad (14)$$

$\dot{\kappa}_s^\alpha$  is the current hardening rate,  $h_0$  is a reference coefficient for hardening,  $\kappa_{s,S}^\alpha$  is the saturation strength value and  $\sum_{\alpha} |\dot{\gamma}^\alpha|$  is accumulated slip.

$\kappa_s^\alpha(t = 0)$  is the critical resolved shear stress (CRSS) of each slip system.  $\kappa_{s,0}^\alpha$ ,  $\kappa_{s,S0}^\alpha$ ,  $\dot{\gamma}_{s,0}^\alpha$  and  $m'$  are other plastic property defining material parameters.

## 2.2 Incorporation of Hydrogen Effects

It has been proposed by Oriani that hydrogen in steel will either reside in normal interstitial lattice sites (NILS) or in traps and remain in equilibrium [26]. It has been discussed previously that diffusion of hydrogen in austenitic stainless steel (FCC) is slow and as such the concentration of hydrogen at material points can be assumed to remain the same during deformation, although there is a transfer of hydrogen atoms from NILS to trap sites [23]. Evidence supporting the constant hydrogen theory has been presented by Schebler [27]. Discussion on the incorporation of hydrogen influence into the model has been discussed previously [23, 28] so only a summary is given here. We express the concentration of hydrogen  $C_{i,bulk}$  at a given material point as

$$C_{i,bulk} = C_L + C_{i,traps} \quad (15)$$

$C_L$  is the concentration in NILS and  $C_{i,traps}$  is the hydrogen in traps before deformation.

Hydrogen in traps  $C_T$  during deformation increases as there is a transfer from  $C_L$  to traps.

$$C_T = \theta_T \psi N_T \quad (16)$$

$\theta_T$  is hydrogen occupancy in traps,  $\psi$  is the number of sites per trap and  $N_T$  represent the number of traps per lattice site.  $N_T$  is:

$$N_T = \frac{\sqrt{3}}{a_{fcc}} \rho \quad (17)$$

$a_{fcc}$  is lattice parameter. Evolution of dislocation density,  $\dot{\rho}$  is:

$$\int_0^t \dot{\rho} dt = (k_1 \sqrt{y}) \int_0^t / \dot{\gamma} / dt \quad (18)$$

$\dot{\gamma}$  is rate of change of strain.  $k_1$  is a measure of immobile dislocations and  $\sqrt{y}$  is the average dislocation separation length as proposed by Estrin et al. [29]. Krom's formulation [30] is used to determine  $C_T$ :

$$C_T = \frac{1}{2} \left[ \frac{N_L}{K_T} + C_{Total} + N_T - \sqrt{\left( \frac{N_L}{K_T} + C_{Total} + N_T \right)^2 - 4N_T C_{Total}} \right] \quad (19)$$

The terms  $H_i$  and  $H_f$  are used to capture the hydrogen effect as previously discussed [23].

$$\kappa_{h,0}^\alpha = \kappa_{s,0}^\alpha * (1 + H_i C_{initial}) \quad (20)$$

$\kappa_{s,0}^\alpha$  is crystal strength with no hydrogen.  $C_{initial}$  is hydrogen traps before plastic deformation and defined as per Caskey's relationship [31];

$$C_{initial} = f C_L e^{18400/(RT)} \quad (21)$$

$f$  is atoms per unit length of dislocation. 18,400 J/mol is bonding energy. Crystal strength evolution in (14) is altered to include hydrogen effect as follows:

$$\dot{\kappa}_s^\alpha = h_0 \left( \frac{\kappa_{s,S}^\alpha - \kappa_s^\alpha}{\kappa_{s,S}^\alpha - \kappa_{s,0}^\alpha} \right) \sum_{\alpha=1}^N |\dot{\gamma}^\alpha| (1 + H_f C_T) \quad (22)$$

Stress triaxiality and Lode parameter are used to quantify stress states [32, 33] as previously discussed by the authors [17]. Lateral displacements are controlled using a multipoint constraint (MPC) subroutine in ABAQUS finite analysis software [34] to keep stress triaxialities and Lode parameter constant at each iteration of the simulations. The relationships in Sects. 2.1 and 2.2 are implemented in a user material subroutine (UMAT) and ABAQUS as discussed in the next chapter.

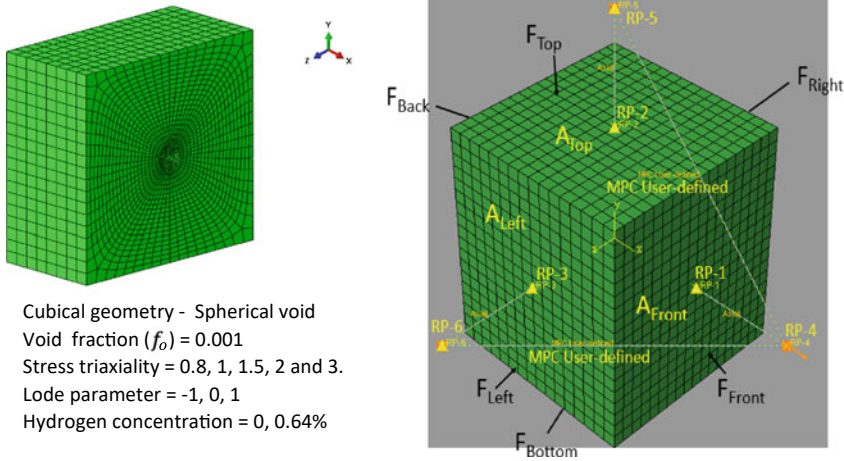
### 3 Methodology

A representative volume element (RVE) is constructed using reduced integrated elements in ABAQUS finite element software. Sample element with an embedded void is shown in Fig. 1 along with the relevant boundary conditions. The embedded void represents a void which has already nucleated as part of the fracture process. The analysis is done using ABAQUS finite element analysis software [34].

The relationship between strain, stress, void growth, void size, stress triaxiality and initial crystal orientation have been covered previously [17, 35]. Only a summary is given here. Void growth is tracked by the term;

$$\text{Normalised void fraction (NVF)} = \frac{f}{f_0}, f = \frac{V_{void}}{V_{RVE}} \quad (23)$$

Initial void volume fraction,  $f_0$  is given by  $(4/3)\pi r^3/s^3$  where  $r$  is sphere radius,  $f$  is void volume fraction, and  $s$  is side length.  $V_{void}$  is the void volume and  $V_{RVE}$  is the sum of solid material and void volume. Loading is done by applying a positive displacement in the  $x$  direction and the sides of the RVE are constraint to remain straight. In Fig. 1,  $F_{Top}$ ,  $F_{Front}$ , and  $F_{Left}$  are mobile while  $F_{bottom}$ ,  $F_{back}$  and  $F_{right}$  are constraint to be fixed during displacement. Lateral displacement is adjusted to keep stress triaxilities constant by applying a multipoint constraint (MPC) subroutine. Using the technique discussed by Tekoglu [36], the stress triaxiality (X) and Lode



Cubical geometry - Spherical void  
 Void fraction ( $f_0$ ) = 0.001  
 Stress triaxiality = 0.8, 1, 1.5, 2 and 3.  
 Lode parameter = -1, 0, 1  
 Hydrogen concentration = 0, 0.64%

**Fig. 1** RVE sample showing boundary conditions

parameter (L) is held constant by satisfying;

$$\rho_{11} = \frac{\sum_{11}}{\sum_{22}}; u_x = \rho_{11} \frac{A_{Front}}{A_{Top}} u_y \tag{24}$$

$$\rho_{33} = \frac{\sum_{33}}{\sum_{22}}; u_z = \rho_{33} \frac{A_{Left}}{A_{Top}} u_y \tag{25}$$

Current RVE volume is

$$V_{RVE} = (s + u_x) * (s + u_y) * (s + u_z) \tag{26}$$

The value of each element ( $V_{e,i}$ ) is stored and summed to obtain

$$V_{solid} = \sum_{i=1}^N V_{e,i} \tag{27}$$

Current value of void volume fraction ( $f$ ) is then obtained by

$$f = \frac{V_{RVE} - V_{solid}}{V_{RVE}} \tag{28}$$

Crystal orientation is represented using Euler angles. Euler angles are three angles used to represent the rotation of an object in space. Here, we have applied the Kock's convention in depicting these angles. Consider a crystal (small cube) shown in relation to a fixed global coordinate axis (big cube) in Fig. 2. We apply a displacement in

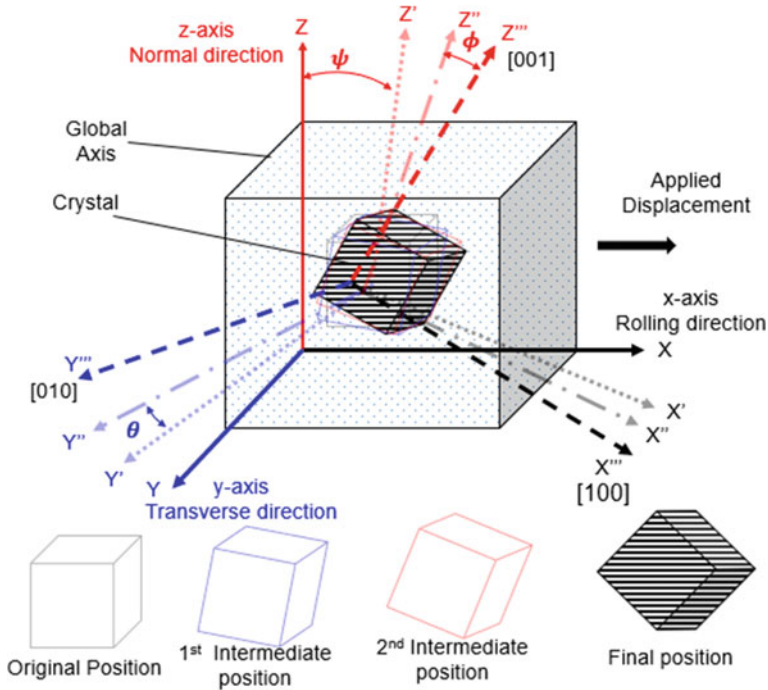


Fig. 2 Representation of crystal orientation in relation to a fixed global axis

the x direction or rolling direction and this impacts the position of the crystal in relation to a fixed global coordinate. The first angle  $\psi$  represents a rotational angle in the z-axis from the original position ( $Z$ ) to a first intermediate position ( $Z'$ ). The second angle  $\theta$  represents rotation and displacement in the y-axis from the first intermediate position ( $Y'$ ) to a second intermediate position ( $Y''$ ). The third angle  $\phi$  represents rotation and displacement in the z-axis from the second intermediate position ( $Z''$ ) to the final position ( $Z'''$ ).

Table 1 summarises the various cases which have been considered. A variety of initial crystal orientations, Lode parameters and stress triaxialities have been considered. However, for the sake of brevity, only selected results (highlighted in light grey) are presented to discuss pertinent findings and observations.

Table 2 shows the various initial crystal orientations and their corresponding stress states. Euler angles in relation to applied displacement considered are illustrated in Fig. 3.

Using the model described, simulations are performed for a range of parameters. Results obtained are discussed in Sect. 4.





**Table 2** Crystal orientations and Euler angles

Euler angles	$\psi$	$\theta$	$\phi$
Orientation 0 (Ori 0)	0°	0°	0°
Orientation A (Ori A)	5°	5°	5°
Orientation B (Ori B)	30°	30°	30°
Orientation C (Ori C)	45°	45°	30°
Orientation D (Ori D)	60°	60°	90°
Orientation E (Ori E)	75°	90°	120°
Orientation F (Ori F)	145°	120°	180°

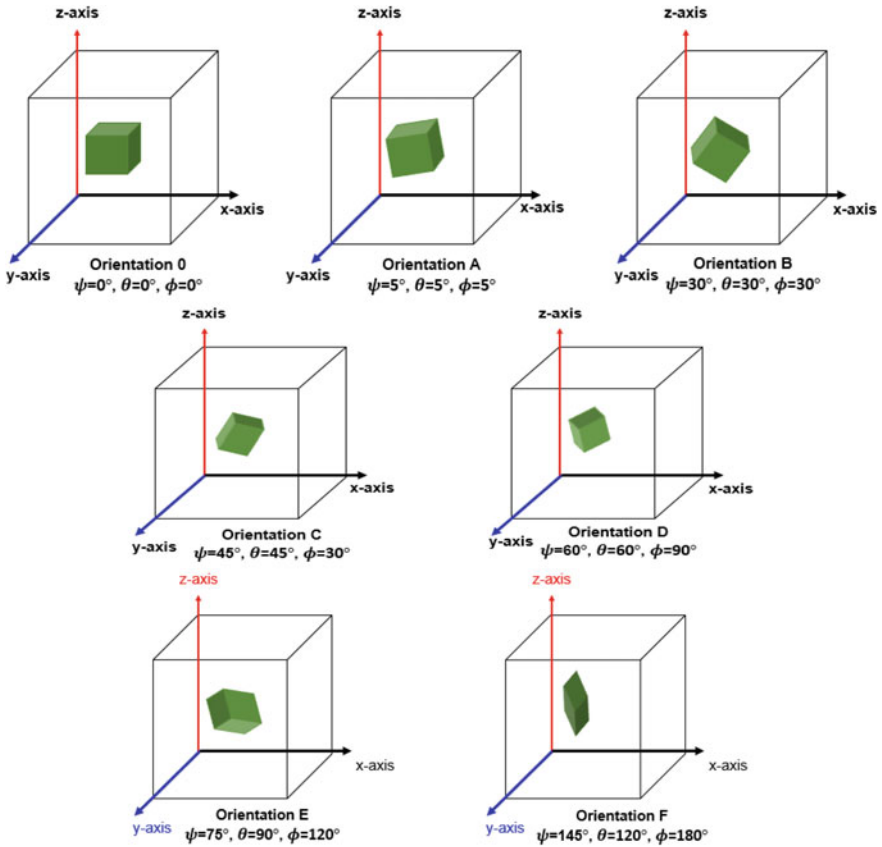


**Fig. 3** Illustration of study cases with initial crystal orientation shown in relation to applied displacement

## 4 Results and Discussion

### 4.1 Effect of Initial Crystal Orientation and Hydrogen on Equivalent Stress

Figure 4 shows the equivalent stress vs equivalent strain curves for different initial crystal orientations. It can be seen that the presence of hydrogen shifts the graph upwards so that the stress value required to transit from elastic to plastic deformation increases. This has been observed previously and is discussed in other works [23, 27]. Table 3 presents an average percentage change equivalent stress due to the presence of hydrogen for the various initial crystal orientations considered. The change in equivalent stress  $\Delta(\sigma)$ (expressed as a percentage) due to hydrogen is computed using the relationship:

$$\Delta(\sigma) = \frac{\sigma_{hydrogen} - \sigma_{Nohydrogen}}{\sigma_{Nohydrogen}} \times 100\% \tag{29}$$

$\sigma_{hydrogen}$  is the average equivalent stress for hydrogenated RVE samples and  $\sigma_{Nohydrogen}$  is the average equivalent stress for non hydrogenated RVE samples.  $\sigma_{hydrogen}$  and  $\sigma_{Nohydrogen}$  are computed up to a equivalent strain value of 0.24 for initial crystal orientations 0, A, B, C, D and E. The maximum equivalent strain obtained for initial crystal orientation F during simulation was 0.155 and values were computed up to this strain.

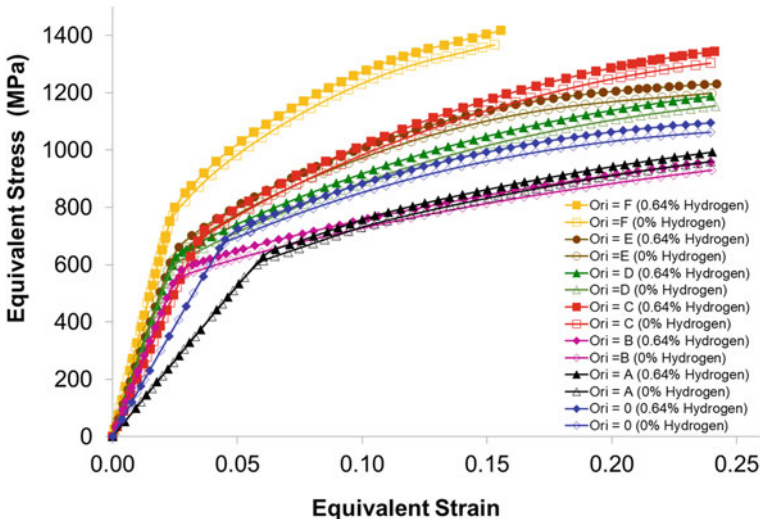


**Fig. 4** Stress strain curves for different initial crystal orientations, viz. stress triaxiality = 1, lode parameter =  $-1$   $f_0 = 0.001$  and hydrogen content = 0.64%

**Table 3** Influence of hydrogen on equivalent stress vs strain relationship at different initial crystal orientations. Stress triaxiality = 1, Lode Parameter =  $-1$   $f_0 = 0.001$  and hydrogen content is 0.64%

	Equivalent stress in (MPa) $\sigma_{hydrogen}$	Equivalent stress (MPa) $\sigma_{No\ hydrogen}$	Change in equivalent stress $\Delta(\sigma)$ (%)	Equivalent strain
Orientation 0 (Ori 0)	987	954	3.52	0.24
Orientation A (Ori A)	856	824	3.94	0.24
Orientation B (Ori B)	665	643	3.38	0.24
Orientation C (Ori C)	1231	1194	3.10	0.24
Orientation D (Ori D)	1055	996	5.84	0.24
Orientation E (Ori E)	1101	1068	3.15	0.24
Orientation F (Ori F)	1221	1181	3.44	0.15

The results show a variation in percentage increase in equivalent stress due to hydrogen of between 3.1% to 5.84% for different initial crystal orientation. The highest change 5.84% was found for initial crystal orientation D (Euler angles  $\psi = 60^\circ$ ,  $\theta = 60^\circ$ ,  $\phi = 90^\circ$ ) and the least change in equivalent was 3.1% for initial crystal orientation C (Euler angles  $\psi = 45^\circ$ ,  $\theta = 45^\circ$ ,  $\phi = 30^\circ$ ). For an initial crystal orientation 0 (Euler angles  $\psi = 0^\circ$ ,  $\theta = 0^\circ$ ,  $\phi = 0^\circ$ ) where the applied direction is perpendicular to the normal, an increase in influence of hydrogen of 3.52% was observed. Initial crystal orientation was found to affect the influence of hydrogen in increasing equivalent stresses and its magnitude differently. Initial crystal orientation was observed to alter the slope of the elastic modulus for both hydrogenated and non hydrogenated samples. As explained elsewhere, plastic work is expended by dislocation activity so hydrogen is not expected to affect elastic modulus [23]. This observation was consistent for a range of stress triaxialities (0.8, 1, 1.5, 2 and 3) and Lode parameters (-1, 0, 1) considered.

#### 4.2 Effect of Initial Crystal Orientation and Hydrogen on Void Growth

Figure 5 shows a variation in the void fraction depending on initial crystal orientations. The results are consistent with the observations reported by Asim et al. [17]. They found that void growth had a strong dependence on initial crystal orientation. Although not clearly observable from the graphs there is a shift in the graph

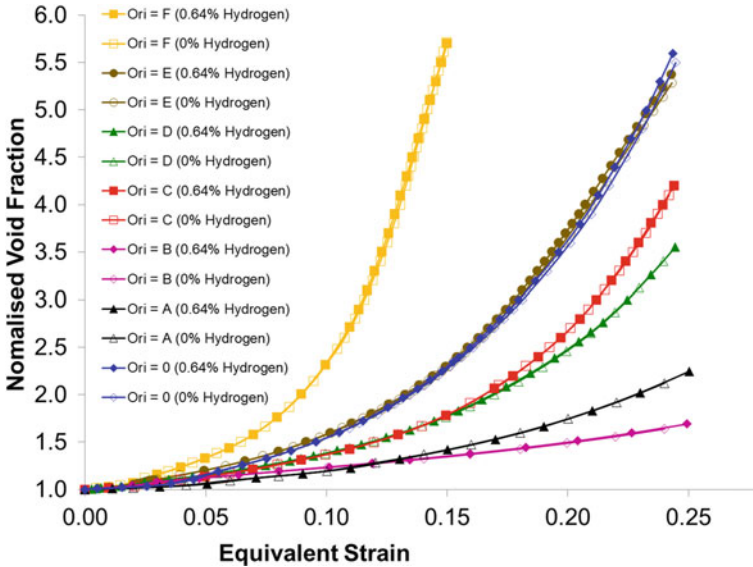


**Fig. 5** Normalised void fraction for different initial crystal orientations, viz. stress triaxiality = 1, lode parameter = -1  $f_0 = 0.001$  and hydrogen content = 0.64%

left for hydrogenated samples which indicates that hydrogen promotes void growth. This has been discussed by the authors elsewhere [28]. Table 4 presents an average percentage change in normalised void fraction due to the presence of hydrogen for the various initial crystal orientations considered. The average change in normalised void fraction  $\Delta NVF$  (expressed as a percentage) due to hydrogen is computed using the relationship:

$$\Delta NVF = \frac{NVF_{hydrogen} - NVF_{No\ hydrogen}}{NVF_{No\ hydrogen}} \times 100\% \tag{30}$$

$NVF_{hydrogen}$  is the average normalised volume fraction for hydrogenated RVE samples and  $NVF_{Nohydrogen}$  is the average normalised volume fraction for non hydrogenated RVE samples.  $NVF_{hydrogen}$  and  $NVF_{Nohydrogen}$  are computed up to a equivalent strain value of 0.24 for initial crystal orientations 0, A, B, C, D and E. The maximum equivalent strain obtained for initial crystal orientation F was 0.155.

The results show a percentage increase in nominal void fraction due to the presence of hydrogen up to 2.7% for different initial crystal orientation. The strongest influence due to hydrogen was 2.7% and this was observed for an initial crystal orientation D (Euler angles  $\psi = 60^\circ, \theta = 60^\circ, \phi = 90^\circ$ ). For an initial crystal orientation 0 (Euler angles  $\psi = 0^\circ, \theta = 0^\circ, \phi = 0^\circ$ ) where the applied displacement direction is penpendicular to the normal, a percentage increase in influence of hydrogen in relation to nominal void fraction was 2.0%. It is noted that the effect of hydrogen

**Table 4** Influence of hydrogen on normalised void fraction at different initial crystal orientations. Stress triaxiality = 1, lode parameter =  $-1$   $f_0 = 0.001$  and hydrogen content is 0.64%

	Normalised void fraction $NVF_{hydrogen}$	Normalised void fraction $NVF_{No\ hydrogen}$	Change in NVF $\Delta NVF$ (%)	Equivalent strain
Orientation 0 (Ori 0)	3.45	3.38	2.0	0.24
Orientation A (Ori A)	1.61	1.60	0.6	0.24
Orientation B (Ori B)	1.25	1.24	0.4	0.24
Orientation C (Ori C)	2.79	2.77	0.7	0.24
Orientation D (Ori D)	2.31	2.24	2.7	0.24
Orientation E (Ori E)	2.61	2.55	2.4	0.24
Orientation F (Ori F)	3.6	3.52	2.3	0.15

varies depending on the initial crystal orientation. This observation was consistent for a range of stress triaxialities (0.8, 1, 1.5, 2 and 3) and lode parameters ( $-1, 0, 1$ ) considered.

### 4.3 Effect of Initial Crystal Orientation on Hydrogen in Traps Distribution During Deformation

To understand the effect of initial crystal orientation on the distribution of hydrogen in traps, contour plots for representative equivalent strains have been derived. Plots of hydrogen in trap distribution for selected equivalent strain values for a variety of initial crystal orientations are shown in Fig. 6. It is observed that the distribution and magnitude of hydrogen in traps had a strong dependence on initial crystal orientation. In all cases considered hydrogen in traps was found to be highest in the immediate vicinity of the void as previously reported [28]. Initial crystal orientations 0, A and B showed a lower maximum value of hydrogen concentrated around the void relative to initial crystal orientations C, D, E and F. A close scrutiny of the Euler angles of these initial crystal orientations, show that initial crystal orientations A and B have a lesser deviation (in terms of Euler angles  $\psi$ ,  $\theta$  and  $\phi$ ) from initial crystal orientation 0 and initial crystal orientations C to F having a higher deviation. The difference in concentration of hydrogen in trap around the void may offer an explanation on the effect initial crystal orientation has on hydrogen influence on local plastic deformation in the area around the void and overall void growth. However, the

relationship between hydrogen in trap concentration around the void and its influence on void growth due to the effect of initial crystal orientation appears to be more complex. As presented in Table 4, initial crystal orientations B reported the lowest change in normalised void fraction compared to other initial crystal orientations (i.e. 0.4%) and also had the least concentration of hydrogen in traps in the vicinity of the void. However, initial crystal orientation C reported a relatively low change in normalised void fraction (i.e. 0.7%), but had a high concentration of hydrogen in trap distribution around the void compared with other cases considered. It is worthwhile

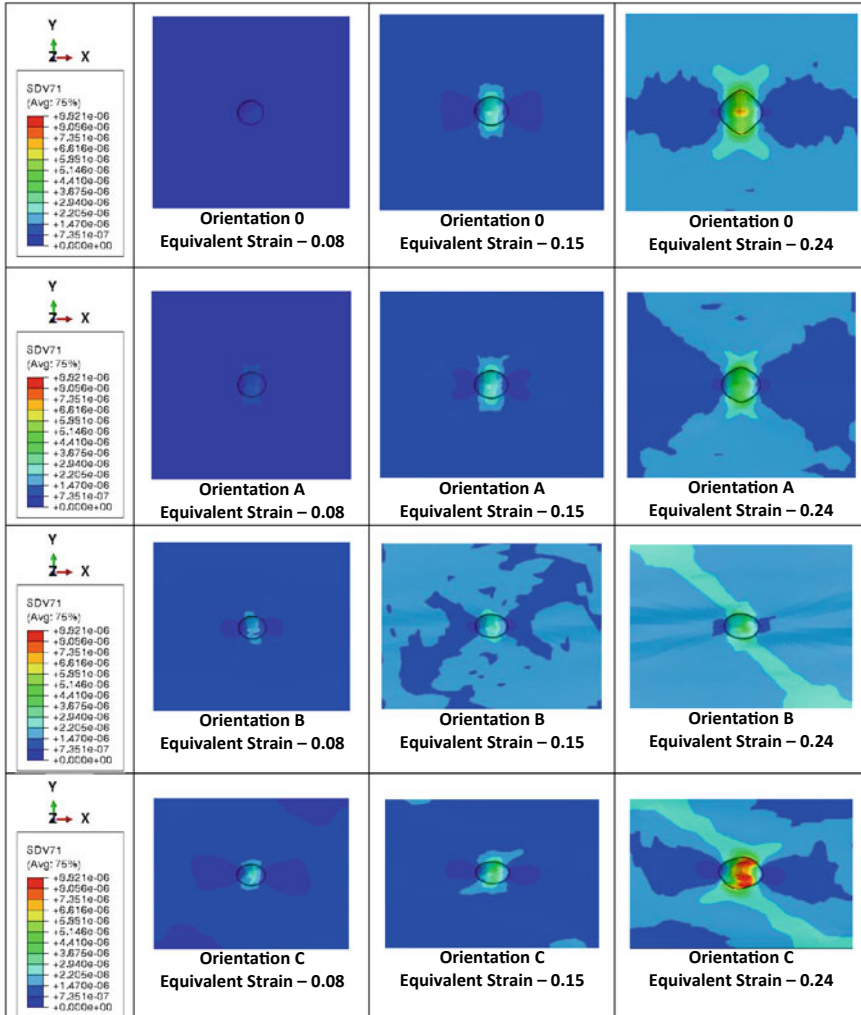


**Fig. 6** Contour plots showing hydrogen in traps distribution for different initial crystal orientations viz. stress triaxiality = 1, lode parameter = -1,  $f_0 = 0.001$  and hydrogen content is 0.64%

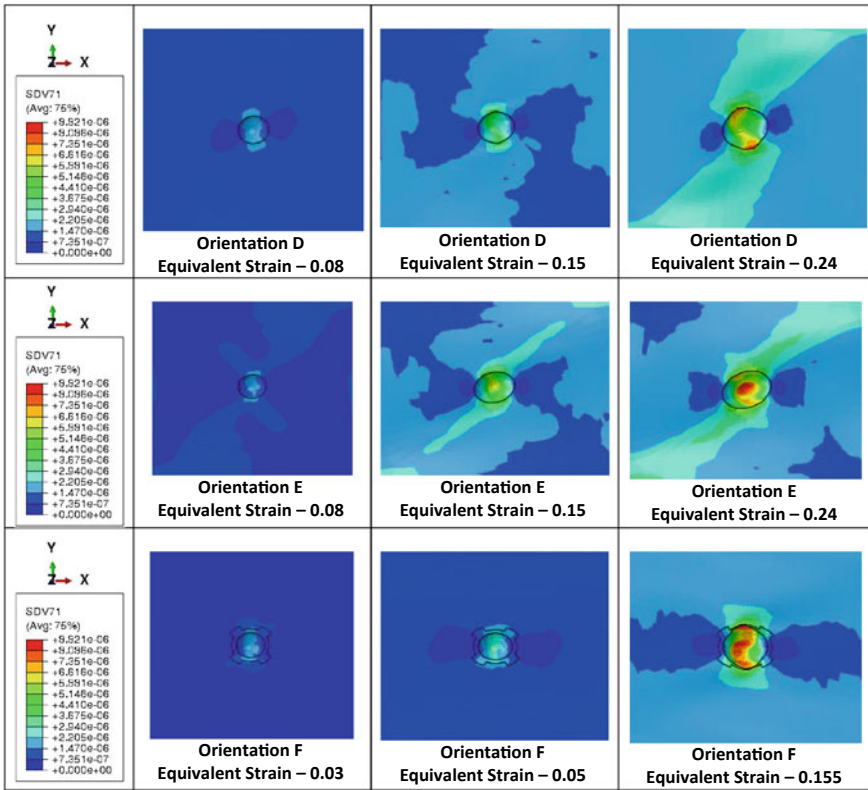


Fig. 6 (continued)

noting that the shape of the voids for the cases considered are varied and this may have an addition effect in void growth evolution if hydrogen influence is affected by void shape.

#### 4.4 Hydrogen in Traps and Slip Activity During Deformation for Different Initial Orientations

Contour plots in Fig. 7 show that slip activity for the various initial crystal orientations follow the same pattern and intensity as the amount of hydrogen in traps presented in Fig. 6. The highest intensity of slip activity was observed in initial crystal orientation C and the intensity in initial crystal orientations 0, A and B were lower than C to F. There is evidence of a strong dependency of initial crystal orientation on the distribution of slip activity which concentrates around the void.



### 4.5 Crystal Orientation Evolution in the Presence of Hydrogen

The evolution of crystal orientation for different stress triaxialities and initial crystal orientations have been studied previously. It was found that the magnitude and direction of crystal rotation was dependent on stress triaxialities and initial crystal orientations [17]. The crystal orientation evolution for hydrogenated and non hydrogenated

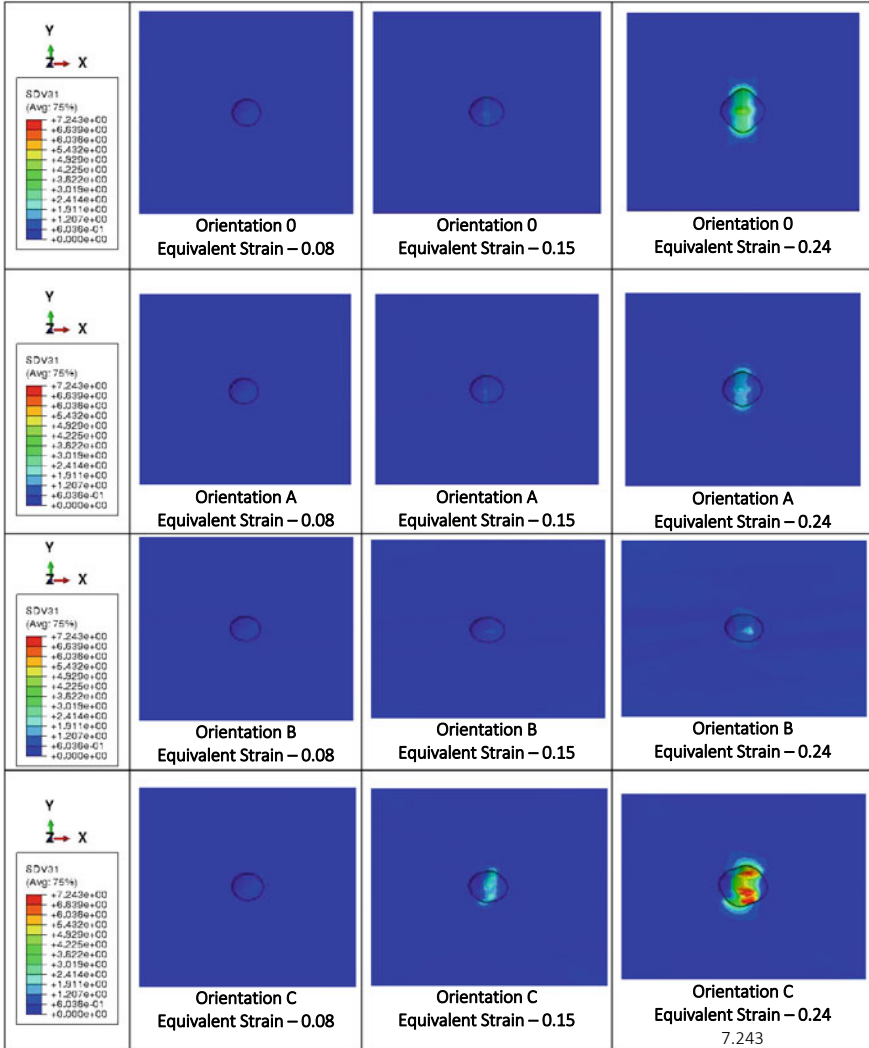


**Fig. 7** Contour plots showing slip activity (SDV31) for different initial crystal orientations viz. stress triaxiality = 1, lode parameter = -1,  $f_0 = 0.001$  and hydrogen content = 0.64%

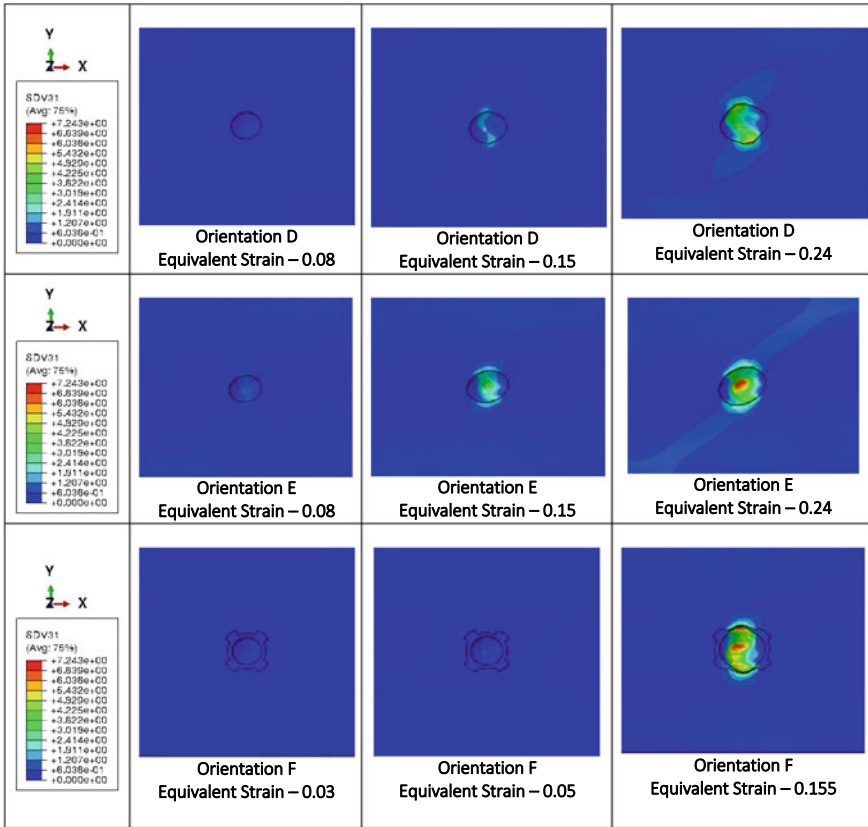
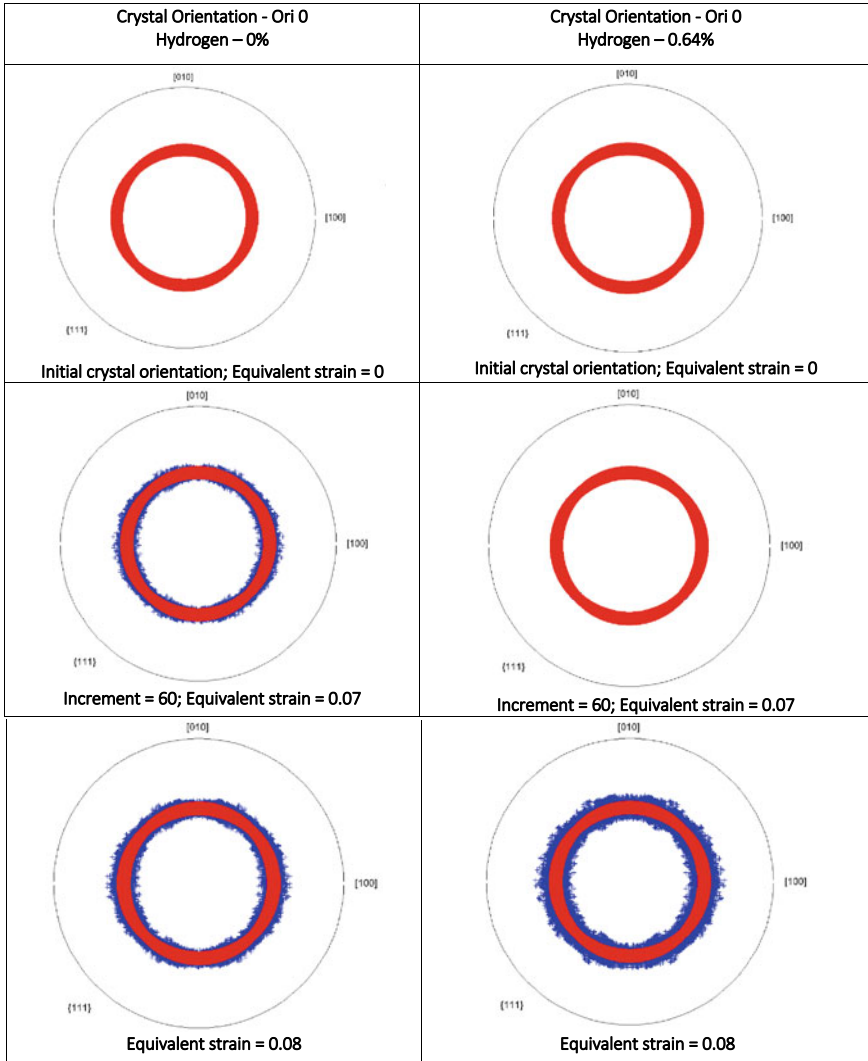


Fig. 7 (continued)

samples have been investigated here. The stress triaxiality and initial crystal orientation are kept the same with RVE samples studied to observe if there are any effect on crystal rotation due to the presence of hydrogen. The pole figures plotted in Fig. 8 show crystal orientation distribution at different stages of the deformation process. It is observed that that presence of hydrogen stifled crystal orientation initially. At an equivalent strain value of 0.07, the RVE sample with no hydrogen show more crystal rotation with respect to the sample exposed to hydrogen indicating this orientation inhibiting effect of hydrogen. However, at an equivalent strain of 0.08, this effect changes and hydrogen appears to encourage crystal orientation. This can be seen as the RVE sample exposed to hydrogen shows more crystal rotation with respect to the sample not exposed to hydrogen. A reference to Figs. 4 and 5 indicate that this change (which occurs around equivalent strain 0.07 and 0.08) position corresponds to the early stages of plastic deformation and steady void growth. This observation show a similar characteristic to previously discussed phenomenon where hydrogen was found to initially impede void growth and beyond a certain equivalent strain value

promote void growth [28]. For equivalent strains 0.09, 0.15 and 0.24, the pole figures show that crystal orientation is largely similar with subtle changes in magnitude. The pattern of crystal rotation remains broadly similar with no significant effect due to hydrogen. It can be inferred that hydrogen has an effect on the evolution of crystal



**Fig. 8** Pole figures showing progression of crystal orientation for hydrogenated and non hydrogenated FCC single crystal viz. stress triaxiality = 1, lode parameter = -1,  $f_0 = 0.001$  and hydrogen content = 0.64%

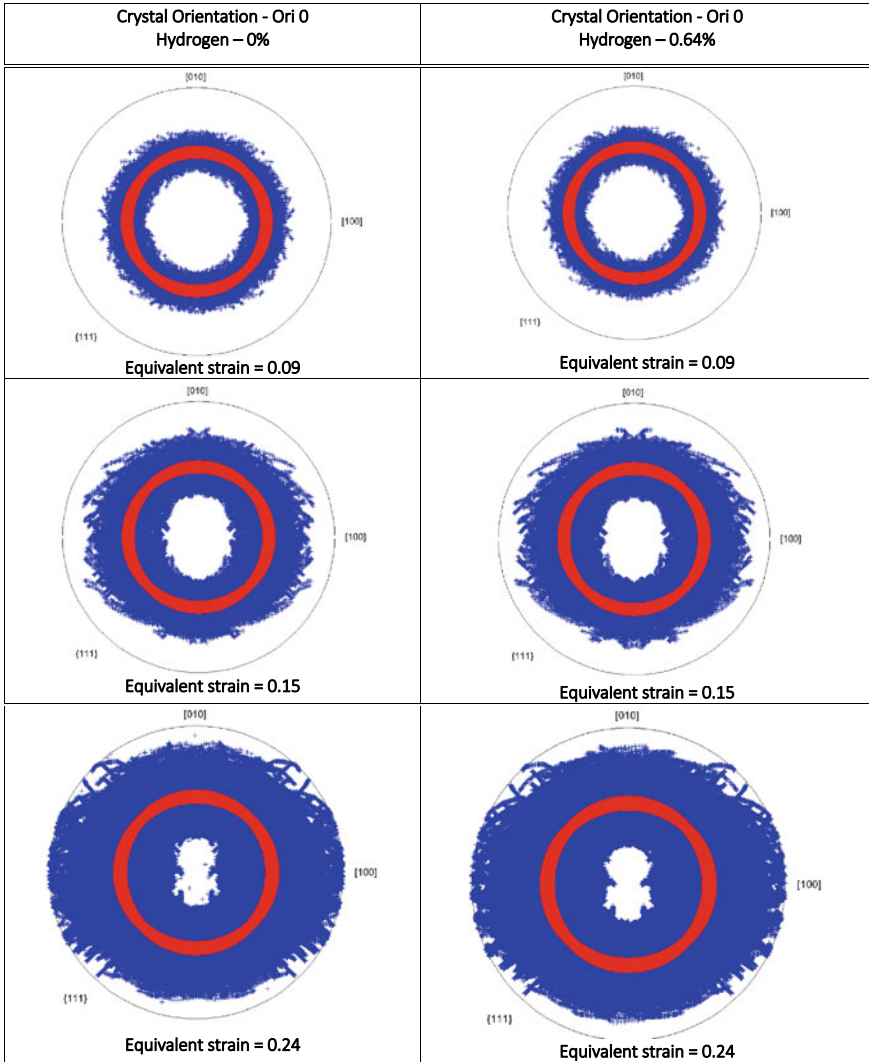


Fig. 8 (continued)

orientation with respect to plastic deformation at the early stages of plastic deformation and void growth. Initially hydrogen is found to impede crystal orientation, but beyond a certain equivalent strain (0.07–0.08 in this study case), this is reversed.

## 5 Conclusions

The effect of crystal orientation on hydrogen influence on void growth in a single crystal of austenitic stainless steel has been studied using a crystal plasticity formulation. There have been finite element based studies into the effect of lattice orientation on void growth without hydrogen influence previously [16, 17] and experimental evidence that hydrogen distribution and mechanisms are affected by crystal orientation [19, 20]. The following conclusions have been drawn from this study:

1. Initial crystal orientation relative to applied displacement is found to affect the influence of hydrogen on plastic deformation and void growth. This effect was found for a variety of stress triaxialities and Lode parameters considered.
2. The distribution and magnitude of hydrogen in traps, especially in the vicinity of the void, was also found to have a strong dependence on initial crystal orientation. The variation in hydrogen in trap distribution around the void provides evidence that there is an effect of initial crystal orientation on hydrogen influence on fracture processes.
3. The evolution of crystal orientation during plastic deformation is affected by the presence of hydrogen although there was no evidence that the general pattern of rotation is significantly affected.

## 6 Future Challenges and Opportunities

The use of models to predict material performance provide the advantage of replicating experimental and real life conditions. Specifically for predicting hydrogen damage, the knowledge of hydrogen transport to the metal surface, entry into the metal, transport within its microstructure, its interaction with crystal defects and microstructure and modification of material properties due to hydrogen are complex phenomena [37] and a good model should account for these. For metals with a FCC crystal structure, it has already been explained that bulk hydrogen transport is limited due to the slow diffusive properties of hydrogen in austenite. For these materials, the interaction of hydrogen with microstructural features and the effects on the material properties is more relevant. A predictive framework based on FEM which incorporates the effects of stress states and crystal orientations for metals with FCC crystal structure will be of practical use to engineers. Suggestion for future work and areas of improvements are as follows:

1. The development of an analytical relationship that captures the effect hydrogen has on fracture processes influenced by strain, stress triaxialities, Lode parameter and crystal orientation will be beneficial.
2. Hydrogen influence is believed to be linked to activation of individual slip systems which occur differently depending on initial crystal orientation. This will have relevance in understanding why certain orientations favour a higher

hydrogen influence on mechanical properties compared with others and should be further investigated.

## References

1. S.I. Wright, D.P. Field, Recent studies of local texture and its influence on failure. *Mater. Sci. Eng. A* **257**(1), 165–170 (1998)
2. V. Venegas, F. Caleyo, T. Baudin, J.H. Espina-Hernández, J.M. Hallen, On the role of crystallographic texture in mitigating hydrogen-induced cracking in pipeline steels. *Corros. Sci.* **53**(12), 4204–4212 (2011)
3. M. Masoumi, C.C. Silva, H.F.G. de Abreu, Effect of crystallographic orientations on the hydrogen-induced cracking resistance improvement of API 5L X70 pipeline steel under various thermomechanical processing. *Corros. Sci.* **111**, 121–131 (2016)
4. T. Graham, On the occlusion of hydrogen gas by metals, *Proc. R. Soc. London*, 422–427 (1868)
5. W. Johnson, On some remarkable changes produced in iron and steel by the action of hydrogen and acids. *R. Soc. London* **14**(2), 168–179 (1874)
6. S.P. Lynch, Progress towards the understanding of mechanisms of hydrogen embrittlement and stress corrosion cracking. *NACE Corros. 2007 Conf. Expo (07493)*, 1–55 (2007)
7. I.M. Robertson, H.K. Birnbaum, P. Sofronis, Hydrogen effects on plasticity **15**(09) (2009)
8. M. Hatano, M. Fujinami, K. Arai, H. Fujii, M. Nagumo, Hydrogen embrittlement of austenitic stainless steels revealed by deformation microstructures and strain-induced creation of vacancies. *Acta Mater.* **67**, 342–353 (2014)
9. Y. Mine, T. Kimoto, Hydrogen uptake in austenitic stainless steels by exposure to gaseous hydrogen and its effect on tensile deformation. *Corros. Sci.* **53**(8), 2619–2629 (2011)
10. P. Birnbaum, H. K., Sofronis, “Hydrogen-enhanced localized plasticity—a mechanism for hydrogen-related fracture,” *Mater. Sci. Eng. A*, vol. 176, no. 1–2, pp. 191–202, 1994.
11. Y. Yagodzinsky, T. Saukkonen, S. Kilpeläinen, F. Tuomisto, H. Hänninen, Effect of hydrogen on plastic strain localization in single crystals of austenitic stainless steel. *Scr. Mater.* **62**(3), 155–158 (2010)
12. Y. Yagodzinsky, E. Malitckii, T. Saukkonen, and H. Hänninen, Hydrogen-induced strain localization in austenitic stainless steels and possible origins of their hydrogen embrittlement, in *2nd International Conference on Metals and Hydrogen*, 2014, May, pp. 203–213 (2014)
13. D.P. Abraham, C.J. Altstetter, Hydrogen-enhanced localization of plasticity in an austenitic stainless steel. *Metall. Mater. Trans. A* **26**(11), 2859–2871 (1995)
14. G.P. Potirniche et al., Role of crystallographic texture on the improvement of hydrogen-induced crack resistance in API 5L X70 pipeline steel. *Int. J. Hydrogen Energy* **42**(3), 14786–14793 (2017)
15. M. Béréš et al., Role of lattice strain and texture in hydrogen embrittlement of 18Ni (300) maraging steel. *Int. J. Hydrogen Energy* **42**(21), 14786–14793 (2017)
16. G.P. Potirniche, J.L. Hearndon, M.F. Horstemeyer, X.W. Ling, Lattice orientation effects on void growth and coalescence in fcc single crystals. *Int. J. Plast* **22**(5), 921–942 (2006)
17. U. Asim, M.A. Siddiq, M. Demiral, Void growth in high strength aluminium alloy single crystals: A CPFEM based study. *Model. Simul. Mater. Sci. Eng.* **25**(3), 035010 (2017)
18. T. Michler, C. San Marchi, J. Naumann, S. Weber, M. Martin, Hydrogen environment embrittlement of stable austenitic steels. *Int. J. Hydrogen Energy* **37**(21), 16231–16246 (2012)
19. Z. Hua, B. An, T. Iijima, C. Gu, J. Zheng, The finding of crystallographic orientation dependence of hydrogen diffusion in austenitic stainless steel by scanning Kelvin probe force microscopy. *Scr. Mater.* **131**, 47–50 (2017)
20. E.G. Astafurova et al., Hydrogen-enhanced orientation dependence of stress relaxation and strain-aging in Hadfield steel single crystals. *Scr. Mater.* **136**, 101–105 (2017)

21. E.B. Marin, On the formulation of a crystal plasticity model. Sandia National Laboratories (2006)
22. A. Siddiq, S. Schmauder, Simulation of hardening in high purity niobium single crystals during deformation. *Steel Grips J. Steel Relat. Mater.* **3**(4), 281–286 (2005)
23. E.I. Ogosi, U.B. Asim, M.A. Siddiq, M.E. Kartal, Modelling hydrogen induced stress corrosion cracking in austenitic stainless steel. *J. Mech.* **36**(2), 213–222 (2020)
24. R. Hill, J.R. Rice, Constitutive analysis of elastic-plastic crystals at arbitrary strain. *J. Mech. Phys. Solids* **20**(6), 401–413 (1972)
25. H.K. Birnbaum, P. Sofronis, Mechanics of the hydrogen-dislocation-impurity interactions-I. Increasing shear modulus. *J. Mech. Phys. Solids* **43**(1), 49–90 (1995)
26. R.A. Oriani, Hydrogen embrittlement of steels. *Annu. Rev. Mater. Sci.* **8**(1), 327–357 (1978)
27. G. Schebler, On the mechanics of the hydrogen interaction with single crystal plasticity. University of Illinois (2011)
28. E. Ogosi, A. Siddiq, U.B. Asim, M.E. Kartal, Crystal plasticity based study to understand the interaction of hydrogen, defects and loading in austenitic stainless steel single crystals. *Int. J. Hydrogen Energy*
29. Y. Estrin, H. Mecking, A unified phenomenological description of work hardening and creep based on one-parameter models. *Acta Metall.* **32**(1), 57–70 (1984)
30. A. Krom, Numerical modelling of hydrogen transport of steel (1998)
31. G.R.J. Caskey, Hydrogen solubility in austenitic stainless steels. *Scr. Metall.* **34**(2), 1187–1190 (1981)
32. T. Luo, X. Gao, On the prediction of ductile fracture by void coalescence and strain localization. *J. Mech. Phys. Solids* **113**, 82–104 (2018)
33. C. Tekoglu, J.W. Hutchinson, T. Pardoen, On localization and void coalescence as a precursor to ductile fracture. *Philos. Trans. R. Soc. A Math. Phys. Eng. Sci.* **373**(2038) (2015)
34. Dassault Systèmes Simulia Corp, “ABAQUS 6.18.” Providence, p. 2018 (2018)
35. U.B. Asim, M.A. Siddiq, M.E. Kartal, Representative volume element (RVE) based crystal plasticity study of void growth on phase boundary in titanium alloys. *Comput. Mater. Sci.* **161**, 346–350 (2019)
36. C. Tekoglu, Representative volume element calculations under constant stress triaxiality, lode parameter, and shear ratio. *Int. J. Solids Struct.* **51**(25–26), 4544–4553 (2014)
37. O. Barrera, D. Bombac, Y. Chen, T.D. Daff, P. Gong, D. Haley, Understanding and mitigating hydrogen embrittlement of steels : a review of experimental, modelling and design progress from atomistic to continuum. *J. Mater. Sci.* **53**(9), 6251–6290 (2018)